Isotopic Enriched and Natural SiC Junction Barrier Schottky Diodes Under Heavy Ion Irradiation

Ketil Røed, Dag Øistein Eriksen, Bruno Ceccaroli, Corinna Martinella, *Member, IEEE*, Arto Javanainen, *Member, IEEE*, Sergey Reshanov, and Silvia Massetti

***Abstract*— The radiation tolerance of isotopic enriched and natural silicon carbide junction barrier Schottky diodes are compared under heavy ion irradiation. Both types of devices experience leakage current degradation as well as single-event burnout events. The results were comparable, although the data may indicate a marginally lower thresholds for the isotopic enriched devices at lower linear energy transfer (LET). Slightly higher reverse bias threshold values for leakage current degradation were also observed compared to previously published work.**

***Index Terms*— Heavy ion irradiation, leakage current degradation, monoisotopic, Schottky diodes, silicon carbide, single-event burnout (SEB), single-event effects.**

I. Introduction

SILICON carbide (SiC) is a wide bandgap semiconductor with favorable material properties for use in power electronics applications. In comparison to silicon, the higher breakdown electric field and thermal conductivity allow SiC devices to operate with higher blocking voltages and at higher temperatures [1], [2]. For SiC power devices, such as high-voltage Schottky diodes and metal oxide semiconductor field-effect transistors (MOSFETs), the build-up of heat can nevertheless lead to reduced material integrity and decreased device performance. The ability to transport heat is therefore an important factor to consider for further development of SiC devices. Studies have shown that isotopic enriched silicon may be one possible way to improve thermal conductivity [3]–[5]. Similar results have also been demonstrated for SiC [6].

Silicon carbide is also an attractive material for power devices used in harsh environments such as space applications. However, SiC power devices are sensitive to particle radiation [7]–[9]. For devices biased in the off state, heavy ion irradiation may result in catastrophic failure such as single-event burnout (SEB), or at voltages below the SEB threshold, leakage current degradation due to multiple single ion strikes. It is suggested that the degradation is caused by local heating effects leading to permanent physical modification of the SiC lattice [8], [10], [11].

Even though it has been shown that isotopic enriched SiC has better thermal conductivity than natural SiC, the consequence of this material property in the performance of electronic devices may be more complex to assess and interpret. Therefore, it is imperative to make electronic components also with pure isotopes and to test them in comparison with the standard devices. This work explores the radiation tolerance between SiC junction barrier Schottky (JBS) diodes manufactured with either natural SiC or isotopic pure SiC, i.e., $^{28}Si^{12}C$, when irradiated with heavy ions at linear energy transfer (LET)-values in SiC of 7.7, 14.5, 25.3, and 49.0 MeV-cm^2/mg. Leakage current degradation and SEB events were observed for both types of devices. The onset of degradation occurred at similar bias voltages for the two higher LET values. At the two lower LET-values, degradation was observed at marginally lower bias voltages for the isotopic enriched devices.

II. Experimental Methods

A. Devices

The devices used for this study were 1.7 kV SiC JBS diodes provided by the Swedish company Ascatron AB (now II-VI Kista AB) – manufactured with either isotopic enriched SiC ($^{28}Si^{12}C$) or natural SiC. Both types use a 355 μm thick substrate of natural SiC manufactured by the Swedish company Norstel (now STMicroelectronics Silicon Carbide AB). On top of these substrates, the University of Linköping (LiU) has grown 100 μm thick epitaxial layers. The configuration of

Manuscript received 11 January 2022; revised 27 February 2022 and 3 April 2022; accepted 3 May 2022. Date of publication 5 May 2022; date of current version 18 July 2022. This work was supported by the General Support Technology Programme (GSTP) European Space Agency (ESA).

The diodes in this study have been produced as part of the Optimal SIC Substrate for Integrated Microwave and Power Circuits (OSIRIS) Project. OSIRIS received funding from the Electronic Component Systems for European Leadership Joint Undertaking (ECSEL JU) under Grant 662322. This JU received support from both the European Union's Horizon 2020 Research and Innovation Program and the Project Participant's National States (France, Norway, Slovakia, and Sweden).

Ketil Røed is with the Department of Physics, University of Oslo, 0316 Oslo, Norway (e-mail: ketil.roed@fys.uio.no).

Dag Øistein Eriksen is with Isosilicon AS, 4622 Kristiansand, Norway, and also with the Department of Chemistry University of Oslo, 0316 Oslo, Norway (e-mail: d.o.eriksen@fys.uio.no).

Bruno Ceccaroli is with Isosilicon AS, 4622 Kristiansand, Norway (e-mail: br-c@online.no).

Corinna Martinella is with the Department of Physics, University of Jyväskylä, 40014 Jyväskylä, Finland, and also with the CERN Engineering Department, 1211 Geneva, Switzerland (e-mail: corinna.martinella@cern.ch).

Arto Javanainen is with the Department of Physics, University of Jyväskylä, 40014 Jyväskylä, Finland, and also with the Electrical Engineering and Computer Science Department, Vanderbilt University, Nashville, TN 37235 USA (e-mail: arto.javanainen@jyu.fi).

Sergey Reshanov is with II-VI Kista AB (former Ascatron AB), 165 40 Kista, Sweden (e-mail: sergey.reshanov@ii-vi.com).

Silvia Massetti is with ESA-ESTEC, 2201 Noordwijk, The Netherlands (e-mail: silvia.massetti@esa.int).

Color versions of one or more figures in this article are available at https://doi.org/10.1109/TNS.2022.3173061.

Digital Object Identifier 10.1109/TNS.2022.3173061

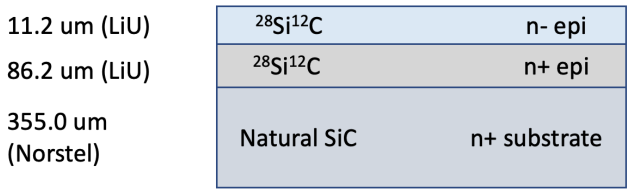

Fig. 1. Layer configuration for isotopic enriched SiC wafer. Image not to scale.

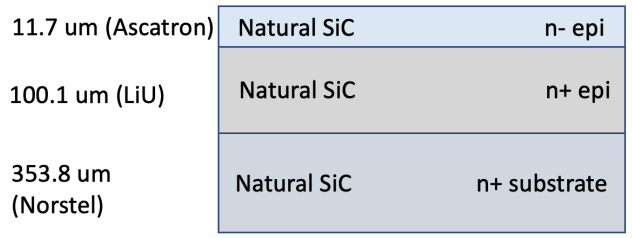

Fig. 2. Layer configuration for natural SiC wafer. Image not to scale.

Fig. 3. Left: Box with bare die diodes, 14 natural SiC, and 14 monoisotopic SiC. Right: Close up of four diodes, bottom right shows cathode/backside, the three others show anode/front side.

TABLE I

OVERVIEW OF PIN AREA GEOMETRIES FOR THE DIFFERENT CONFIGURATIONS

Configuration	PiN geometry [μm^2]	Total PiN area [μm^2]	PiN area / anode area [%]
A	900 x 900	(620 000 + 810 000)	20
B-1	300 x 320	(620 000 + 864 000)	20
B-2	300 x 535	(620 000 + 1 444 500)	28

these layers is illustrated in Fig. 1 for the isotopic enriched wafer and in Fig. 2 for the natural wafer. For one wafer, the epitaxial layer was enriched with ^{28}Si- and ^{12}C-isotopes, and contained both the n+ buffer and a 11.2 μm n-drift layer. On the second wafer, an epitaxial layer of natural SiC was grown containing only the n+ buffer. A 11.7 μm n-drift layer was then grown on top of the latter by Ascatron AB. The device active layers were grown by chemical vapor deposition (CVD). Growth occurred at elevated temperatures (1500 °C–1700 °C) with hydrogen as a carrier gas with precursors and dopants. Either silane (SiH_4) or trichlorosilane (TCS) were used as a silicon precursor; as a carbon precursor of either ethene or propane was used. Nitrogen gas was used for n-doping. All p+ areas (anode and termination) were fabricated by Al implantation (at 500 °C) and followed by high-temperature annealing (1650 °C in Ar).

TABLE II

SPECIFICATIONS OF JBS SiC DIODES. THE BLOCKING VOLTAGE IS THE VOLTAGE AT WHICH THE REVERSE BIAS LEAKAGE CURRENT, I_R, IS EXPECTED TO BE LOWER THAN OR EQUAL TO 0.1 mA

Parameter	Type/Conditions	Value
Blocking voltage	$I_R \leq$0.1 mA	1.7 kV
Forward current, I_F	V_F=1.8V	20 A
Die size		3.3 x 3.3 mm^2
Anode contact size		2.7 x 2.7 mm^2
Epitaxial depth (n-drift)	isotopic / natural	11.2 / 11.7 μm
Termination width	Floating rings	150 μm
Polyimide passivation	PI2611	5.7 μm
Anode metallization	TiW / Al (100 %)	0.12 / 4.0 μm
Cathode metallization	Ti / Ni / Ag	0.06 / 0.5 / 1.0 μm
Polytype	4H-SiC	
Doping n-drift	natural	$7.7 \cdot 10^{15}$ cm^{-3}
Doping n-drift	isotopic	$7.5 \cdot 10^{15}$ cm^{-3}
Doping n+buffer	natural	$1.5 \cdot 10^{18}$ cm^{-3}
Doping n+buffer	isotopic	$1.2 \cdot 10^{18}$ cm^{-3}

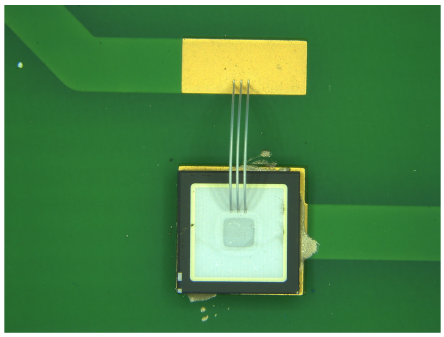

Fig. 4. Diodes were mounted directly on PCBs (cathode side down) using conductive silver epoxy. The anode side is connected to a nearby pad using three ⌀ 25 μm aluminum bonding wires, each expecting to support approximately 0.75 A. The bonding wires are assumed to be sufficiently thin to disregard beam shadowing effects.

The diodes were provided as bare dies in two groups: 14 diodes of natural SiC (labeled *n1 – n14*) and 14 diodes (labeled *i1 – i14*) of isotopic pure SiC (^{28}Si and ^{12}C), see Fig. 3. The slightly darker structures seen inside the anode area in the right image of Fig. 3, are PiN areas for surge current capability. Ascatron has provided diodes with two different configurations for the PiN areas, either a larger square area (configuration A), or nine smaller rectangular areas (configuration B). For configuration B, two slightly different geometries were used. An overview of the different configurations is shown in Table I. Besides the visible central PiN areas, all diodes have PiN rings around the device edge of 10 μm width and several 8 μm feeders across, adding 620 000 μm^2 to the total PiN area. The fraction of the total PiN area to the total anode area is 20% for configuration A and B-1, and 28% for configuration B-2. P+-rings are used for electric field termination purposes and placed outside the active area. They are floating and not participating in the current conduction. The active area of the diodes is protected by a 4 μm Al layer. Other relevant diode parameters are listed in Table II.

B. Test Setup

The devices were bonded on custom printed circuit boards (PCBs) as shown in Fig. 4: three boards with eight

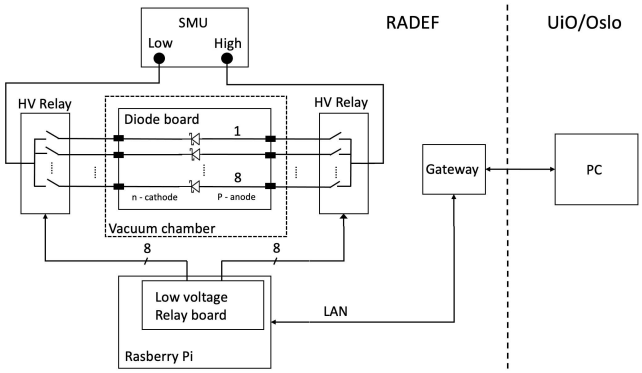

Fig. 5. Schematic overview of the measurement setup at RADEF. The setup was controlled remotely from Oslo.

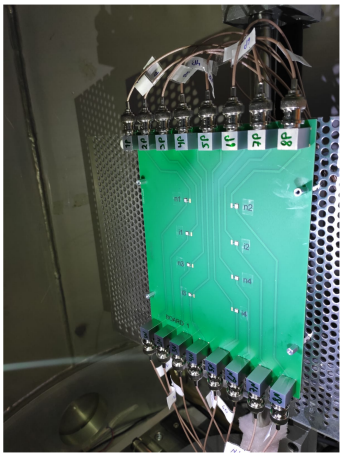

Fig. 6. Board 1 with eight diodes mounted in the RADEF vacuum chamber.

TABLE III
CHARACTERISTICS OF THE ION BEAMS USED AT RADEF. THE VALUES FOR AVERAGE LET AND PROJECTED RANGE ARE ESTIMATED USING [12], DESCRIBED IN [13]

Ion	Energy [MeV]	LET(SiC) @ surface [MeV-cm^2/mg]	Range in SiC [μm]
$^{40}Ar^{14+}$	657	7.7	177
$^{57}Fe^{20+}$	941	14.5	139
$^{83}Kr^{29+}$	1358	25.3	126
$^{126}Xe^{44+}$	2059	49.0	113

diodes, one board with four diodes, and each board with an equal number of isotopic enriched and natural-type devices. The diodes are separated by a minimum distance of 3 cm, and the PCB is coated with 16 μm of parylene to prevent electrical arcing.

A Keithley 2410 1100 V source measure unit (SMU) was used to source the bias voltage and to measure the current of the diodes. The Keithley 2410 has a current limit of 1 A below 20 V and 20 mA between 20 and 1100 V. A high current breakdown event would therefore bring the SMU into compliance at 20 mA. The connection from the SMU to a diode was established through two custom made high-voltage relay boards. The Keithley's high-side output was connected to the diode's anode side, while the low-side return was connected to the diode's cathode side. A Raspberry Pi 4 was used to control the individual high-voltage relays using another commercial add-on low-voltage relay board. The terminals of all the diodes not under test are unconnected and floating. A schematic overview of the test setup is shown in Fig. 5. The Raspberry Pi was connected to the local area network and a remote connection to Oslo was established through a gateway. The measurements were controlled from Oslo due to the Covid-19-related travel restrictions at the time of testing.

To qualify the diodes for irradiation, their leakage currents were monitored for 96 h at a reverse bias of -1000 V. Forward and reverse bias sweeps were performed before and after this test. Devices that showed significant changes in leakage current or sweep characteristics were disqualified for irradiation. The qualification measurements were performed at room temperature enclosed in an aluminum box.

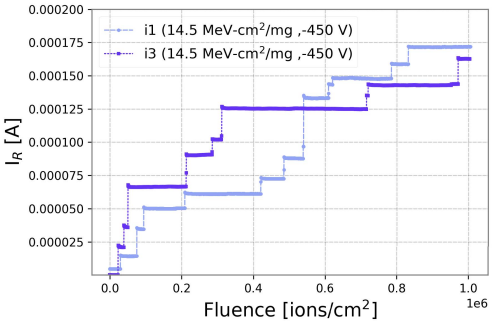

Fig. 7. Example showing discrete heavy ion-induced steps in the leakage current during irradiation at -450 V for devices *i1* and *i3* at an ion LET of 14.5 MeV-cm^2/mg.

C. Test Conditions

The heavy ion irradiations were performed using the 16.3 MeV/n cocktail at the radiation effects facility (RADEF) in the Accelerator Laboratory of the University of Jyväskylä [14]. The irradiations were performed at normal incidence to the device surface with the ion beam characteristics listed in Table III. A circular collimator ($\varnothing$ 2 cm) was used to limit the beam size and expose only one device at the time. The devices were irradiated to a target fluence of 10^6 ions/cm^2, with fluxes ranging from 500 ions/(cm^2-s) to 10 000 ions/(cm^2-s), adopted according to the device response. For all devices, forward and reverse bias sweeps were performed before irradiation and after each irradiation step. All measurements were performed at room temperature and in vacuum conditions. Fig. 6 shows one of the PCBs mounted in the RADEF vacuum chamber.

Four devices, two of each type, were tested for each ion LET, starting at the lowest value. For each ion LET, the reverse bias was incremented in regular steps to identify the threshold for heavy ion leakage current degradation or SEB events. To further narrow down the threshold, the bias voltage step size was then reduced prior to reaching this value when testing the second device.

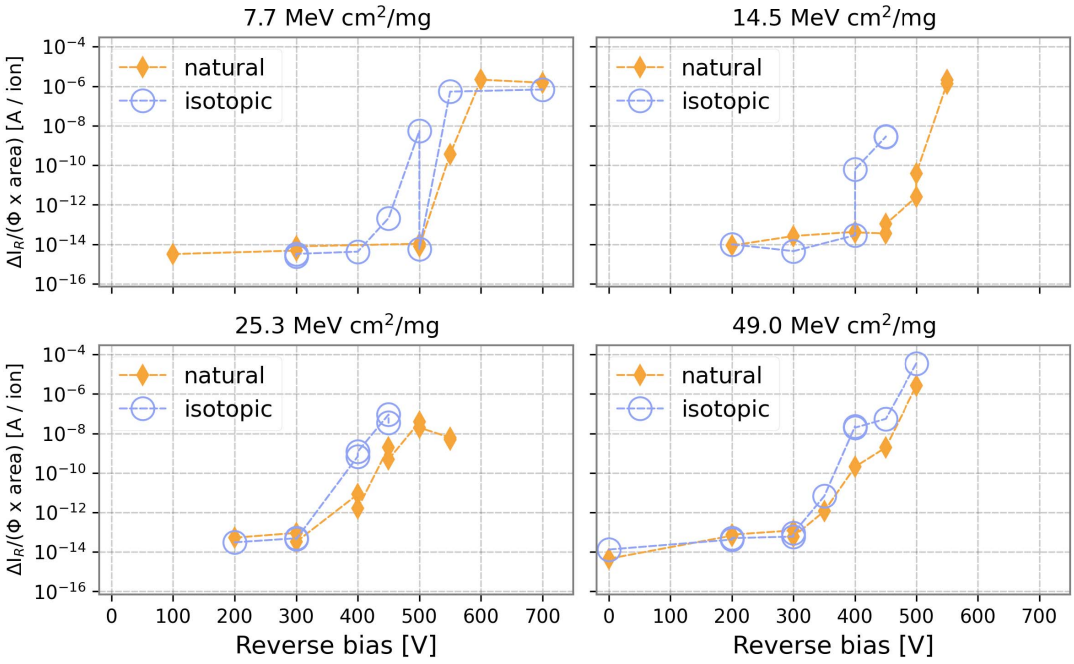

Fig. 8. Change in heavy ion-induced leakage current as a function of the reverse bias voltage applied during irradiation for isotopic enriched and natural-type devices. Each point corresponds to an individual diode measurement. The values are normalized to the fluence and the Schottky area of the diodes. The target fluence for all runs were $1 \cdot 10^6$ ions/cm^2. However, a few runs reached a lower fluence due to device failure (e.g., SEB).

III. Results

A. Leakage Current Degradation

Leakage current degradation was observed for both types of devices for all LET-values.

Fig. 7 shows an example of discrete heavy ion-induced steps for devices *i1* and *i3* exposed to an LET of 14.5 MeV-cm^2/mg at −450 V.

To further analyze the onset of degradation, Fig. 8 shows the change in leakage current ($\Delta I_R/(\Phi \times \text{area})$) as a function of reverse bias and LET. This is calculated by subtracting the current measured immediately before irradiation from the current measured immediately after irradiation (ΔI_R). To account for the small variation in PiN areas for some of the diodes and to any differences in beam exposure, the values are normalized to the Schottky area and fluence (Φ) for that run. The normalization to the area has a negligible influence on the results—the trend remained the same with or without the normalization.

No leakage current degradation was observed up to 300 V for any of the devices. That is, the measured current was similar before and after the irradiation. At 7 MeV-cm^2/mg, a significant change was first observed at a reverse bias voltage of 450 V for the isotopic type and at 550 V for the natural type. A slightly lower threshold was also seen for the isotopic type at 14.5 MeV-cm^2/mg. For the two higher LET values, the threshold was observed at the same reverse bias voltage for both types. The discrepancy in the two values measured for the isotopic type at 7.7 MeV-cm^2/mg and −500 V is likely due to the low occurrence of ion-induced leakage current degradation at this LET-value. No degradation step was observed for one of the devices at −500 V although a single step was seen for the same device at −450 V. Similarly, at 14.5 MeV-cm^2/mg and −400 V, one of the two devices did not experience any degradation for this or previous test conditions.

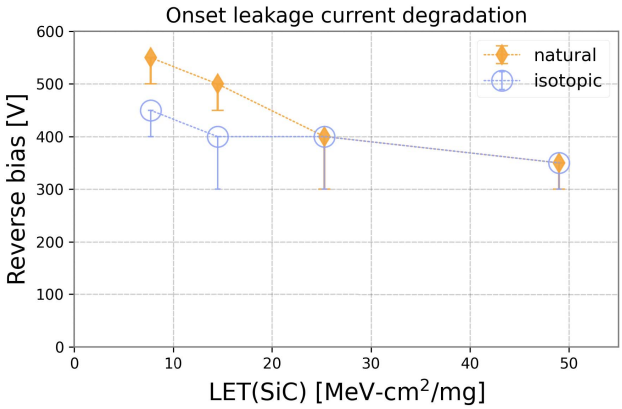

Fig. 9. Reverse bias voltage at which degradation was first observed during irradiation as function of ion LET for isotopic enriched and natural-type devices. Errorbars extend to the highest bias value at which no degradation was measured.

As also observed by others [10], [15], [16], the threshold for degradation is dependent on both the bias voltage and ion LET. The results are summarized in Fig. 9 where the reverse bias voltage at which degradation was first observed during irradiation is plotted as a function of ion LET. While the results are comparable for both types of devices, the data may indicate a marginally lower threshold for leakage current degradation during irradiation for the isotopic enriched type at the two lower LET values.

B. Postirradiation I–V

Forward and reverse bias sweeps were performed after each irradiation step. For some devices, a change in the

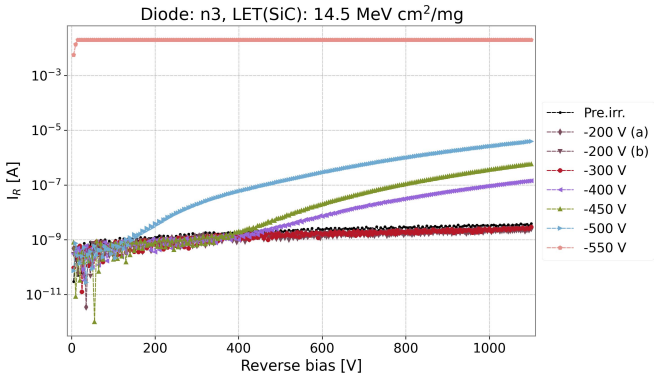

Fig. 10. Example showing reverse bias sweeps for device n3 which was irradiated at an LET of 14.5 MeV-cm^2/mg. The values listed in the legend correspond to the reverse bias voltages applied during the irradiation performed just before the I-V-measurements. *Pre.irr.* refers to the I–V-measurement performed before the device was irradiated. Two consecutive I–V-measurements were performed after the −200 V run.

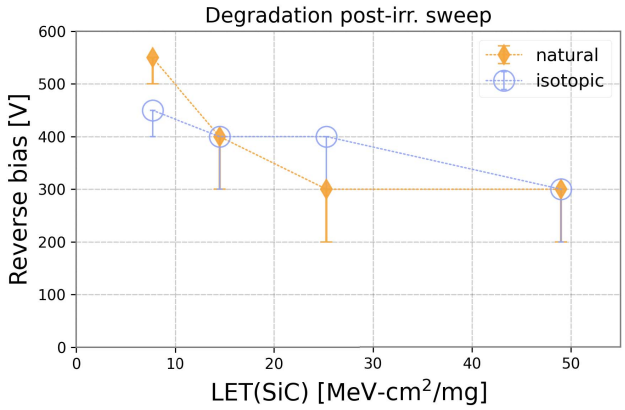

Fig. 11. Reverse bias voltage (during irradiation) at which a significant change was observed in the postirradiation I–V-characteristics. The data are plotted as a function of ion LET for isotopic enriched and natural-type devices. Errorbars extend to the highest bias value at which no degradation was measured.

I–V-characteristics was observed although no leakage current degradation was detected during irradiation. An example can be seen in Fig. 10 for device *n3* at 14.5 MeV-cm^2/mg. While no leakage current degradation was seen during irradiation below −500 V, the reverse I–V-curve deviates from the preirradiation measurement already after being irradiated at −400 V. For all devices where this behavior was seen, the I–V-curve started to deviate at reverse bias values above or close to the value applied during irradiation. The deviation from the preirradiation measurement indicates that the devices may already have experienced minor degradation during the corresponding irradiation run, but that the heavy ion-induced steps possibly were too small to be detected with the applied measurement setup.

Fig. 11 shows for which reverse bias voltage applied during irradiation, a significant change was first seen in the postirradiation I–V-characteristics. The trend is similar to the data shown in Fig. 9: decreasing threshold with increasing LET. On the other hand, the marginal difference seen between the isotopic type and the natural type at the two lower LET values is washed out.

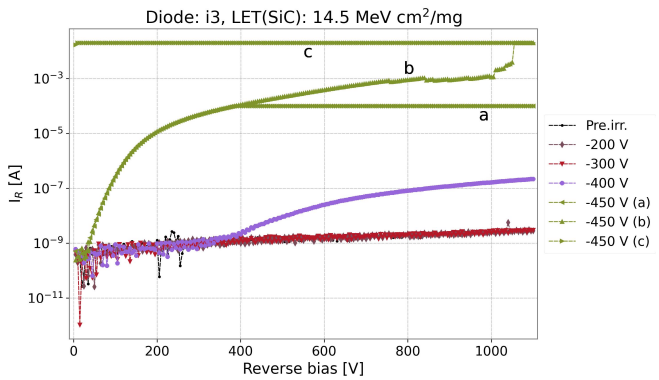

Fig. 12. Example showing reverse bias sweeps for device i3 which was irradiated at an LET of 14.5 MeV-cm^2/mg. The values listed in the legend correspond to the reverse bias voltages applied during the irradiation performed just before the I–V-measurements. *Pre.irr.* refers to the I–V-measurement performed before the device was irradiated. Three consecutive I–V-measurements were performed after the −450 V run.

Device *n3* experienced an SEB event during irradiation when exposed to −550 V. The postirradiation I–V-curve clearly shows how the reverse leakage current reached the 20 mA compliance level of the SMU. For some devices, breakdown occurred already during the postirradiation sweep. The combination of accumulated degradation during irradiation and the additional stress applied during a sweep to high bias values, may eventually cause the device to break down before reaching the nominal breakdown voltage. An example can be seen in Fig. 12 for device *i3* at 14.5 MeV-cm^2/mg. After the device has been irradiated at −450 V the first postirradiation sweep (labeled a in the figure) saturated at 0.1 mA due to an incorrectly set current limit of the SMU. When the current limit was removed, a clear step in the I–V-curve is seen around 1050 V (b). A third sweep confirmed the breakdown both in the reverse and forward sweep.

Notice that device *n3* does not experience break down during the postirradiation sweep—even after being irradiated at higher reverse bias voltages compared to device *i3*. In fact, the same behavior was also observed between the two other devices irradiated at 14.5 MeV-cm^2/mg: devices *n7* and *i1*. While the isotopic type devices broke down during the postirradiation sweep, and therefore could not be used to further test for SEB, the natural-type devices did not. Again, this may indicate that the isotopic devices are marginally more sensitive. A similar comparison could not be done for 7.7 MeV-cm^2/mg due to the incorrect current limit only discovered when testing at 14.5 MeV-cm^2/mg, and consequently removed after this. It is in fact likely that this current limit allowed the devices tested at 7.7 MeV-cm^2/mg to reach the appropriate condition to trigger an SEB. The current limit was only applied for the I–V-measurements and not during irradiation.

C. SEB

Prior damage caused by leakage current degradation makes it difficult to evaluate the threshold for SEB [8], [10]. In this work, SEB events were only observed for devices with minor prior leakage current degradation, and where the devices did not break during the postirradiation sweep. At low ion LET,

TABLE IV

RANGE FOR SEB THRESHOLD. THE HIGH-SIDE IS THE BIAS AT WHICH SEB WAS MEASURED, AND THE LOW-SIDE IS THE HIGHEST VALUE AT WHICH NO SEB WAS OBSERVED. THE RANGE IS BASED ON MEASUREMENTS OF THE SAME DEVICE, EXCEPT FOR THE POINT AT 49 MeV-cm^2/mg. A DASH INDICATES THAT NO SEB WAS MEASURED FOR THIS LET

	LET(SiC) [MeV-cm^2/mg]			
	7.7	14.5	25.3	49.0
n	550–600 V	500–550 V	-	-
i	500–550 V	-	-	450–500 V

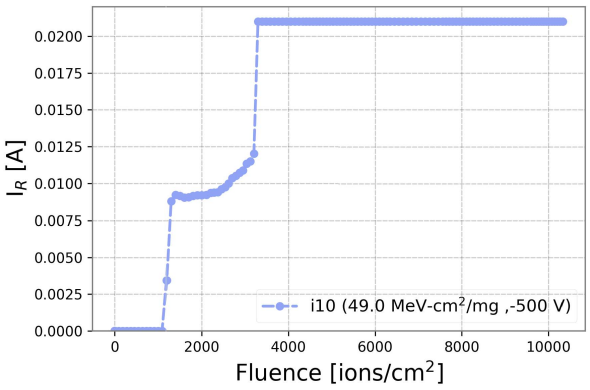

Fig. 13. Example of an SEB event for device i10 for an ion LET of 49.0 MeV-cm^2/mg at −450 V.

typically only a few degradation steps were observed before an SEB event occurred. However, as the ion LET was increased, a significant increase in leakage current into the μA–mA range was observed, likely damaging the devices already before reaching the SEB threshold. Based on the measurements, suggested ranges for the SEB threshold are listed in Table IV. These ranges correspond to 26%–35% of the devices' blocking voltage, comparable to values reported in [16]. The 49.0 MeV-cm^2/mg point is based on measurements with two pristine devices. One device (*i10*) was tested directly at a reverse bias of 500 V without any prior exposure. As can be seen in Fig. 13, an SEB was observed only a few seconds after the beam was turned on at a flux of 1000 ions/(cm^2-s). Decreasing the reverse bias voltage, another device (*i11*) was then tested at 450 V. The measurement in Fig. 14 shows a rapid increase in the current immediately after the beam is turned on, before finally saturating just above 3 mA. These two measurement results indicate that the SEB threshold may lie in the range 450–500 V for the isotopic type at 49 MeV-cm^2/mg. It should also be noted that although device *i11* reached the compliance level of the SMU above 600 V during the I–V-measurement, the forward characteristic was still normal. Similar behavior was seen for several devices at the two higher LET values, and for repeated consecutive I–V-measurements, indicating that a full breakdown has not occurred.

Similar to the leakage current degradation, the results may indicate a marginally lower SEB threshold for the isotopic enriched type at 7.7 MeV-cm^2/mg. However, due to the testing methodology, focusing on leakage current degradation, any difference in SEB threshold could not be investigated for the higher LET values. Testing for SEB should therefore ideally be done with pristine devices, starting from a high bias and decreasing until SEBs are no longer observed. If postirradiation I–V-characteristics are required, an appropriate current limit should also be considered.

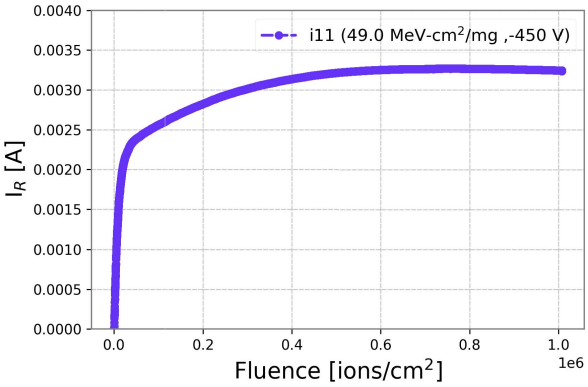

Fig. 14. Example of significant increase in leakage current for device i11 for an ion LET of 49.0 MeV-cm^2/mg at −450 V.

IV. DISCUSSION

There are two main observations in this work: first, while the results are comparable for both types of devices, the data may indicate marginally lower thresholds for the isotopic type at 7.7 and 14.5 MeV-cm^2/mg; second, the threshold voltage for leakage current degradation appears to be slightly higher than previously published literature [16], [17].

For each ion LET, the data are based on only two devices. This is a clear limitation, which given the results make it difficult to form a confident conclusion. Nevertheless, the leakage current degradation rate is observed to be systematically higher for the isotopic pure devices for all LETs, although marginally. At 14.5 MeV-cm^2/mg the results also indicate that the isotopic devices have become more susceptible to breakdown during postirradiation I–V-measurements. Again, the data are limited, but at least these different measurements are all in disfavor of the isotopic device.

There are minor differences in how the two types of devices are manufactured. The n-drift layers have been grown at two different facilities. While the breakdown voltage depends on both the thickness of the n-drift layer and its doping levels, the values are still relatively comparable between the two types. Also, the breakdown voltage is generally considered to increase with increasing n-drift layer thickness and decreasing doping. A slight decrease in doping level for the isotopic device and a slight increase in the n-drift thickness for the natural type may cancel out any difference.

In [17], it is also suggested that the degradation threshold is independent of device parameters, including the breakdown voltage and the epitaxial depth and doping density. Fig. 1 in [17] shows a leakage current degradation plot for a wide range of rated breakdown voltage (600–1700 V) which all have similar thresholds. The thickness of the n-drift layer for the tested devices' range from 3.7 to 14 μm, and are in line with the isotopic and natural devices tested in this work. Similar results can also be seen in Fig. 2 in [16]

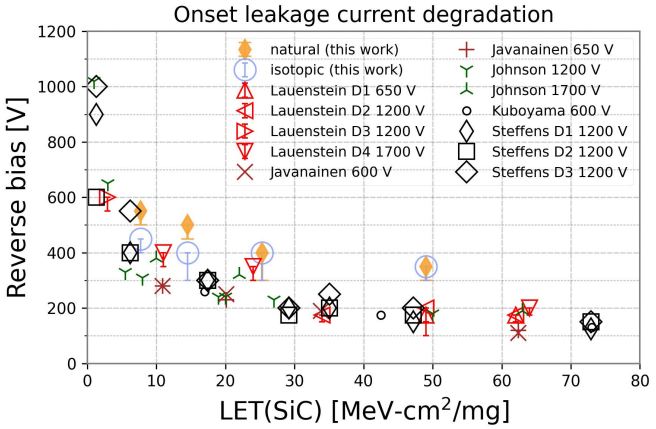

Fig. 15. Data from the measurements in this work are compared to data from work done by from Kuboyama *et al.* [8], Javanainen *et al.* [10], Lauenstein *et al.* [16], Johnson *et al.* [17], and Steffens *et al.* [18]. The values are estimated from the plots in [16]– [18]. For [18], the data from the Université catholique de Louvain (UCL) and the Grand Accélérateur National d'Ions Lourds (GANIL) are used – errorbars are not provided, and it is assumed that the data points correspond to the onset of leakage current degradation. In [16], the values include similar errorbars to the data in this work, extending down to the highest voltage at which no leakage current degradation occurred. For the remaining works, the data are plotted as the average between the lowest voltage at which no leakage current degradation was observed and the lowest voltage at which leakage current degradation occurred.

were both Schottky barrier diodes (SBDs) and junction barrier diodes (JBS) were tested, and in [18] for three different Schottky diodes. The data from [17]—including therein also data from [10] and [8]—and from [16] and [18], are compared to the results in this work in Fig. 15.

For the measurement points at 49 MeV-cm^2/mg, the threshold voltages measured for the devices in this work are 100–150 V higher compared to previously published work. The trend is also slightly higher for the natural type at the lower LET values, expect maybe for the D3 device at around 6 MeV-cm^2/mg in [18]. If the work in [17] suggests an independence on voltage rating, n-drift layer thickness, and doping level, the higher threshold measured for this work may suggest another cause.

Carriers generated during an ion strike generate a uniform localized conductive path across the n-drift layer resulting in a resistive shunt across the device, and consequently power dissipation. As shown in [17] and [19], this low-resistance path is not a linear resistor over the entire drift region. A peak in the power density is seen near the contact region and where the n-drift layer meets the highly doped substrate. The peak in the electric field at the n-drift/n+ interface is also higher than the electric field required for avalanche breakdown, which generates additional carries that can contribute to device damage.

In [20], simulations shows that reducing the substrate doping level by a factor of two (from $5{\cdot}10^{18}$ cm^3 to $2.5 \cdot 10^{18}$ cm^3) can reduce the maximum temperature in the thermal transient following the ion impact. A decrease in doping level increases the substrate resistance, which behaves like a resistance in series with the shunt resistance, and may therefore reduce the current flowing through the device. Both types of devices in this work have been manufactured with an additional $\sim$100 μm n+ buffer layer with a doping level of $\sim 1{\cdot}10^{18}$ cm^3, see Table II. This is different from many devices where the n-drift layer is usually grown directly on a highly doped substrate. Information about doping levels for commercial devices are not always available. Still, information from [11] and [20] suggests that the doping levels for the n+ buffer in this work is on the lower side.

In [21], a study showed that the addition of a buffer layer between the n-drift layer and substrate of power depletion MOSFETs (DMOSFETs) can improve a device's SEB tolerance. Adding a buffer layer changes the electric field distribution, which results in a lower maximum electric field, and consequently a higher SEB breakdown voltage. The peak of the electric field shifts from the n-drift/n+ buffer to the n+ buffer/substrate interface. These two effects can be seen when comparing Figs. 1 and 2 in [21]. Quasi-stationary avalanche simulations also shows that the choice of buffer resistivity and thickness is important. It is suggested that an optimum value exist and that a too low or high resistivity and/or too thick or thin buffer layer is less effective. No specific values are given for the resistivity and buffer layer thickness in [21], but the figures suggest that the thickness is comparable to or a bit thinner than the n-drift layer.

A further improvement can be achieved by introducing a linear doped buffer layer as demonstrated through simulations in [22], where the doping concentration is changed linearly over a 10 μm buffer layer. This resulted in a lower peak electric field compared to a constant doping buffer layer.

The studies performed in [20]– [22] show that the substrate doping and the design of the interface between the n-drift and substrate is important for the electric field power density distribution. While these studies focused on SEB, their results are also likely relevant for leakage current degradation. For the isotopic and natural-type devices in this work, the n+ buffer is a constant doping layer with a doping level of a few 10^{18} cm^{-3}. Fig. 5 in [22], indicates that doping levels lower than $\sim 10^{17}$ cm^{-3} may be required to significantly alter the electric field distribution. Furthermore, the n+ buffer in this study is thicker than in the above-mentioned studies. However, since the n-drift layer was manufactured in two different facilities, potential differences in the epi growth process may have resulted in different transient doping profile between the n-drift and n+ buffer—effectively introducing a thinner buffer region potentially behaving as shown in [21] and [22]. Also, the interruption in the growth process for the natural device, where the n+ buffer was grown at LiU and the n-drift layer was grown at Ascatron, may have introduced additional defects in the n+ buffer/n-drift junction. While these differences may be small, they could play a role in explaining the difference observed between the natural and isotopic type devices. And the effect may be less pronounced at the higher LET value where the power densities quickly rise above the threshold for leakage current degradation. This may further point to the added and slightly lower doped n+ buffer layer as the main reason for the improved threshold compared to previously published work.

The ranges of the particle beams used in this study are comparable to the depth of the n+ buffer/n+ substrate interface.

However, the resistance in the n+ buffer is still significantly lower compared to the n-drift region. The electric field will therefore mainly be distributed across the $\sim$11 μm drift region where the ion track will induce the low resistance shunt—and where the ion LET will remain relatively constant. Charge deposited in the n+ buffer region is likely of less importance.

V. Conclusion

Heavy ion irradiation has been performed on isotopic enriched and natural SiC JBS diodes. Both types of diodes experience leakage current degradation and SEB events. The results are comparable for both types of devices, although the data may indicate marginally lower thresholds for the isotopic type. The devices are manufactured with an additional n+ buffer with slightly lower doping levels than usual for substrates; and the n-drift layer for the two types has been grown at two different facilities. This n+ buffer and its interface to the n-drift layer may play a role in explaining the differences observed between the isotopic and natural types. It may also contribute to the slightly higher reverse bias threshold voltage measured compared to other works. With the current design and manufacturing process, we can conclude that a device with isotopic enriched SiC did not provide an evident advantage with respect to leakage current degradation and SEB, but that the importance of the n+ buffer layer must be further studied.

Acknowledgment

The authors would like to thank Optimal SIC Substrate for Integrated Microwave and Power Circuits (OSIRIS) research consortium under Electronic Component Systems for European Leadership Joint Undertaking (ECSEL JU) and particularly Ascatron AB (now II-IV Kista AB) among the consortium's partners for providing diodes and invaluable information. The help from the staff at Laboratory for electronics (ELAB) at the Department of Physics, UiO, with printed circuit board (PCB) design and bonding of diodes is greatly appreciated. Berget AS is acknowledged for performing the parylene coating of the diode PCBs. They would also like to thank the Radiation Effects Facility (RADEF) Group at the Accelerator Laboratory of the University of Jyväskylä for their great support and for providing the opportunity to perform remote testing. The Norwegian Space Agency deserves acknowledgments for facilitating the collaboration and contract with the European Space Agency.

References

[1] A. Elasser and T. P. Chow, "Silicon carbide benefits and advantages for power electronics circuits and systems," *Proc. IEEE*, vol. 90, no. 6, pp. 969–986, Jun. 2002.

[2] J. Millan, P. Godignon, X. Perpina, A. Perez-Tomas, and J. Rebollo, "A survey of wide bandgap power semiconductor devices," *IEEE Trans. Power Electron.*, vol. 29, no. 5, pp. 2155–2163, May 2014.

[3] R. K. Kremer *et al.*, "Thermal conductivity of isotopically enriched ^{28}Si: Revisited," *Solid State Commun.*, vol. 131, no. 8, pp. 499–503, Aug. 2004.

[4] A. V. Gusev, A. M. Gibin, O. N. Morozkin, V. A. Gavva, and A. V. Mitin, "Thermal conductivity of ^{28}Si from 80 to 300 K," *Inorg. Mater.*, vol. 38, no. 11, pp. 1100–1102, 2002.

[5] A. V. Inyushkin *et al.*, "Ultrahigh thermal conductivity of isotopically enriched silicon," *J. Appl. Phys.*, vol. 123, no. 9, Mar. 2018, Art. no. 095112.

[6] B. Lundqvist *et al.*, "Thermal conductivity of isotopically enriched silicon carbide," in *Proc. 19th Workshop Thermal Invest. ICs Syst. (THERMINIC)*, Berlin, Germany, Sep. 2013, pp. 58–61.

[7] S. Kuboyama, C. Kamezawa, Y. Satoh, T. Hirao, and H. Ohyama, "Single-event burnout of silicon carbide Schottky barrier diodes caused by high energy protons," *IEEE Trans. Nucl. Sci.*, vol. 54, no. 6, pp. 2379–2383, Dec. 2007.

[8] S. Kuboyama, C. Kamezawa, N. Ikeda, T. Hirao, and H. Ohyama, "Anomalous charge collection in silicon carbide Schottky barrier diodes and resulting permanent damage and single-event burnout," *IEEE Trans. Nucl. Sci.*, vol. 53, no. 6, pp. 3343–3348, Dec. 2006.

[9] E. Mizuta, S. Kuboyama, H. Abe, Y. Iwata, and T. Tamura, "Investigation of single-event damages on silicon carbide (SiC) power MOSFETs," *IEEE Trans. Nucl. Sci.*, vol. 61, no. 4, pp. 1924–1928, Aug. 2014.

[10] A. Javanainen *et al.*, "Heavy ion induced degradation in SiC Schottky diodes: Bias and energy deposition dependence," *IEEE Trans. Nucl. Sci.*, vol. 64, no. 1, pp. 415–420, Jan. 2017.

[11] A. F. Witulski *et al.*, "Single-event burnout of SiC junction barrier Schottky diode high-voltage power devices," *IEEE Trans. Nucl. Sci.*, vol. 65, no. 1, pp. 256–261, Jan. 2018.

[12] A. Virtanen, H. Kettunen, A. Javanainen, and M. Rossi. *RADiation Effects Facility at JYFL*. Accessed: Oct. 6, 2021. [Online]. Available: http://www.jyu.fi/accelerator/radef

[13] A. Javanainen. (2015). *European Component Irradiation Faciliteis Cocktail Calculator*. Accessed: Oct. 6, 2021. [Online]. Available: http://research.jyu.fi/radef/ECIFcalc/index.html

[14] A. Javanainen, "A simple expression for electronic stopping force of heavy ions in solids," *Nucl. Instrum. Methods Phys. Res. B, Beam Interact. Mater. At.* vol. 285, pp. 158–161, Aug. 2012.

[15] C. Martinella *et al.*, "Current transport mechanism for heavy-ion degraded SiC MOSFETs," *IEEE Trans. Nucl. Sci.*, vol. 66, no. 7, pp. 1702–1709, Jul. 2019.

[16] J.-M. Lauenstein, M. C. Casey, R. L. Ladbury, H. S. Kim, A. M. Phan, and A. D. Topper, "Space radiation effects on SiC power device reliability," in *Proc. IEEE Int. Reliab. Phys. Symp. (IRPS)*, Mar. 2021, pp. 498–506.

[17] R. A. Johnson *et al.*, "Unifying concepts for ion-induced leakage current degradation in silicon carbide Schottky power diodes," *IEEE Trans. Nucl. Sci.*, vol. 67, no. 1, pp. 135–139, Jan. 2020.

[18] M. Steffens, S. K. Höffgen, T. Kündgen, E. Paschkowski, M. Poizat, and D. Wölk, "Single event sensitivity and de-rating of SiC power devices to heavy ions and protons," in *Proc. Radiat. Effects Data Workshop (RADECS)*. Montpellier, France, Sep. 2019, pp. 1–5. Accessed: Oct. 6, 2021. [Online]. Available: http://publica.fraunhofer.de/documents/N-572145.html

[19] D. R. Ball *et al.*, "Ion-induced energy pulse mechanism for single-event burnout in high-voltage SiC power MOSFETs and junction barrier Schottky diodes," *IEEE Trans. Nucl. Sci.*, vol. 67, no. 1, pp. 22–28, Jan. 2020.

[20] C. Abbate *et al.*, "Analysis of heavy ion irradiation induced thermal damage in SiC Schottky diodes," *IEEE Trans. Nucl. Sci.*, vol. 62, no. 1, pp. 202–209, Feb. 2015.

[21] S. Liu, J. L. Titus, and M. Boden, "Effect of buffer layer on single-event burnout of power DMOSFETs," *IEEE Trans. Nucl. Sci.*, vol. 54, no. 6, pp. 2554–2560, Dec. 2007.

[22] Y. Jia, H. Su, R. Jin, D. Hu, and Y. Wu, "Simulation study on single event burnout in linear doping buffer layer engineered power VDMOSFET," *J. Semiconductors*, vol. 37, no. 2, Feb. 2016, Art. no. 024008.